

## Impacts of organic aerosols and its oxidation level on CCN activity from measurement at a suburban site in China

Fang Zhang<sup>1,2</sup>, Zhanqing Li\*<sup>1,2,3</sup>, Yanan Li<sup>1,2</sup>, Yele Sun<sup>4</sup>, Zhenzhu Wang<sup>5</sup>, Ping Li<sup>1,2</sup>,

Li Sun<sup>6</sup>, Maureen Cribb<sup>3</sup>, Chuanfeng Zhao<sup>1,2</sup>, Qingqing Wang<sup>4</sup>

5 <sup>1</sup>State Key Laboratory of Earth Surface Processes and Resource Ecology, College of Global Change and Earth System Science, Beijing Normal University, Beijing 100875, China

<sup>2</sup>Joint Center for Global Change Studies, Beijing 100875, China

10 <sup>3</sup>Earth System Science Interdisciplinary Center and Department of Atmospheric and Oceanic Science, University of Maryland, College Park, Maryland, USA.

<sup>4</sup>State Key Laboratory of Atmospheric Boundary Layer Physics and Atmospheric Chemistry, Institute of Atmospheric Physics, Chinese Academy of Sciences, Beijing 100029, China

15 <sup>5</sup>Key Laboratory of Atmospheric Composition and Optical Radiation, Anhui Institute of Optics and Fine Mechanics, Chinese Academy of Sciences, Hefei 230031, China

<sup>6</sup>Liaoning Weather Modification Office, Shenyang, 112000, China

\*correspondence to: Z. Li (zli@atmos.umd.edu)

20

## Abstract

This study is concerned with the impacts of organic aerosols on CCN activity based on field measurements made at a suburban site in north China. The sensitivity of volume fraction of organic aerosols ( $x_{org}$ ) as well as oxidation level (using  $f_{44}$ , the fraction of m/z 44 in total organics, as an indicator) of organics on estimating  $N_{CCN}$  is examined. A strong dependence of CCN number concentration ( $N_{CCN}$ ) on the  $x_{org}$  and  $f_{44}$  was noted. The sensitivity of volume fraction of organics to  $N_{CCN}$  increased with increasing  $x_{org}$ . The impacts of the aerosol particles oxidization or aging level on estimating  $N_{CCN}$  were also very significant. When the particles were mostly composed of organics ( $x_{org}>60\%$ ), the  $N_{CCN}$  at the supersaturation of 0.075% and 0.13% was underestimated by 46% and 44% respectively if aerosol particles were freshly emitted with primary organics ( $f_{44}<11\%$ ); while the underestimation decreased to 32% and 23% at the corresponding supersaturations if the particles were with more hygroscopic secondary organics ( $f_{44}>15\%$ ). The  $N_{CCN}$  at the supersaturation of 0.76% was underestimated by 11% and 4% respectively at  $f_{44}<11\%$  and  $f_{44}>15\%$ . But for the particles composed of low organics (e.g.  $x_{org}<40\%$ ), the effect caused by the  $f_{44}$  was quite insignificant both at high and low supersaturations. This is due to that the overall hygroscopicity of the particles is dominated by inorganics such as sulfate and nitrate, which are more hygroscopic than organic compounds. Our results indicated that it would decrease the uncertainties in estimating  $N_{CCN}$  and lead to a more accurate estimation of  $N_{CCN}$  to increase the proportion of secondary organics, especially when the composition of the aerosols is dominated by organics.

The applicability of the CCN activation spectrum obtained at Xinzhou to the Xianghe site, about 400 km to the northeast of Xinzhou, was investigated, with the aim of further examining the sensitivity of CCN to aerosol type. Overall, the mean CCN efficiency spectrum derived from Xinzhou performs well at Xianghe when the supersaturation levels are  $> 0.2\%$  (overestimation of 2-4%). However,  $N_{\text{CCN}}$  was overestimated by  $\sim 20\%$  at supersaturation levels of  $< 0.1\%$ . This suggests that the overestimation is mainly due to the smaller proportion of aged and oxidized organic aerosols present at Xianghe compared with Xinzhou.

## 9 **1. Introduction**

10 To reduce the uncertainty of aerosol indirect effects on the radiative balance of  
11 the atmosphere, it is important to gain a good knowledge of the ability of aerosol  
12 particles to form cloud condensation nuclei (CCN) at the typical supersaturations  
13 found in the atmosphere. The CCN activity of aerosol particles is governed by the  
14 Köhler theory (Köhler, 1936). This theory determines CCN from aerosol particle size  
15 and physicochemical properties, which include the molar volume, activity coefficient,  
16 and effect on surface tension (McFiggans et al., 2006). These properties, however, are  
17 difficult to measure.

18 Researchers have proposed single-parameter models to parameterize the CCN  
19 activation and hygroscopicity of multi-component aerosols (Hudson and Da, 1996;  
20 Rissler et al., 2006; Petters and Kreidenweis, 2007; Wex et al., 2007). Field  
21 experiments have been conducted with the aim of better characterizing particle  
22 physicochemical parameters influencing cloud CCN activation. Due to the large  
23 spatial variability of aerosol types and compositions, the CCN activation efficiency  
24 varies greatly over different regions. CCN number concentrations ( $N_{\text{CCN}}$ ) can often be  
25 better predicted in the background atmosphere (Chuang et al., 2000; Dusek et al.,  
26 2003; VanReken et al., 2003; Rissler et al., 2004; Gasparini et al., 2006; Stroud et al.,  
27 2007; Bougiatioti et al., 2009).

28 The largest errors are associated with urban emissions (Sotiropoulou et al., 2007).  
29 This is likely due to the organics component of aerosol particles, which have the  
30 largest uncertainty and are not fully understood. Biomass burning aerosols and  
31 secondary organics formed from the oxidation of common biogenic emissions are  
32 often more difficult to activate (Mircea et al., 2005; VanReken et al., 2005; Lee et al.,  
33 2006; Varutbangkul et al., 2006; Clarke et al., 2007; Rose et al., 2010; Engelhart et al.,

2012; Paramonov et al., 2013; Lathem et al., 2013; Mei et al., 2013b; Zhang et al., 2014). Particles with aged/oxidized secondary organic components (e.g., organic acids) have been shown to be more hygroscopic (Raymond and Pandis, 2002; Hartz et al., 2006; Bougiatioti et al., 2011), but still much less hygroscopic than inorganic species. The sensitivity of estimated  $N_{CCN}$  to organics have been examined in a number of recent studies (Wang et al., 2008; Reutter et al., 2009; Ervens et al., 2010; Kammermann et al., 2010; Ward et al., 2010; Zhang et al., 2012; Mei et al., 2013a). It is widely known that the estimated  $N_{CCN}$  is sensitive to changes in organics due to the latter's complex components. The amounts and hygroscopicity parameter of organics ( $\kappa_{org}$ ) vary substantially and lead to significant biases in estimating CCN concentrations and aerosol indirect forcing (Sotiropoulou et al., 2007; Hings et al., 2008; Liu and Wang, 2010). Therefore, field investigations regarding CCN activity and organics impacts, especially in heavily polluted regions, are pivotal to better parameterize CCN in climate models.

Northern China is a fast developing and densely populated region of China, where aerosol loading is high (Li et al., 2007, 2011), the particle composition is complex, and severe haze pollution episodes are common (Guo et al., 2014). In recent years, CCN measurements have been collected during field campaigns carried out in the region (Wiedensohler et al., 2009; Gunthe et al., 2011; Yue et al., 2011; Deng et al., 2011, 2013; Zhang et al., 2014). These studies have presented different perspectives on the influence of particle size and composition on CCN activity. For example, Deng et al. (2013) evaluated various schemes for CCN parameterization and recommended that the particle number size distribution (PSD) together with inferred mean size-resolved activation ratios can be used to estimate CCN number concentrations without considering the impact of particle composition. However,

59 Zhang et al. (2014) demonstrated that the 30–40% uncertainties in  $N_{CCN}$  are mainly  
60 associated with changes in particle composition. None of the above-mentioned studies  
61 have investigated the impact of organics on estimating  $N_{CCN}$  in Northern China.  
62 Zhang et al. (2012) noted a more significant influence of organics on CCN activity but  
63 without concerning the influences of particles oxidation or aging on CCN activity; in  
64 addition, the campaign average mass fraction of organics in their study was < 20%.

65 The aim of this paper is to examine the sensitivity of changes in aerosol  
66 physicochemical properties (especially aerosols containing large amounts of organics,  
67 as well as the oxidation level) to CCN activity, and also to see how much uncertainty  
68 is incurred by applying the CCN efficiency spectra measured at one site to another  
69 site in a heavily polluted region. The instrumentation and data used in the study are  
70 described in section 2. The method for calculating the hygroscopicity parameter ( $\kappa_{chem}$ )  
71 is introduced in section 3. The sensitivity of  $x_{org}$  as well as oxidation level of organics  
72 on estimating  $N_{CCN}$  in section 4, and the ability of the CCN efficiency spectrum  
73 observed at the Xinzhou site to represent CCN at the Xianghe site, are also presented  
74 and discussed at the last part of this section. Conclusions from the study are given in  
75 section 5.

## 76 2. Measurements and data

77 An intensive observation period field campaign similar to the  
78 Aerosol-CCN-Cloud Closure Experiment (Zhang et al., 2014), called the Atmosphere,  
79 Aerosol, Cloud, and CCN ( $A^2C^2$ ) experiment, was conducted from 22 July to 26  
80 August of 2014 at Xinzhou (38.24°N, 112.43°E; 1500 m above sea level), a city with a  
81 population of 0.51 million in Northern China. The site is located about 360 km  
82 southwest of the metropolitan Beijing area and about 10 km south of the local town  
83 center. The site is surrounded by agricultural land (e.g., corn) with little local pollution

84 plums from motor vehicles and industrial activities. Sitting between two mountains  
85 (Taihang Mountain to the east and Lüliang Mountain to the west), the site also  
86 experiences air masses from Xinzhou City to the north and from Taiyuan City to the  
87 south, the capital of Shanxi Province. Air masses from the northeast and southwest  
88 dominate over the site during summer. Depending on the wind direction,  
89 measurements at the Xinzhou site can detect air parcels of urban, rural, or mixed  
90 origins, including both fresh biogenic emissions around the site and aged aerosols  
91 from advection.

## 92 **2.1 Instruments and measurements**

93 During the field campaign, a Scanning Mobility Particle Sizer (SMPS),  
94 combined with a Droplet Measurement Technologies-Cloud Condensation Nuclei  
95 Counter (DMT-CCN<sub>C</sub>) (Lance et al., 2006), was used for size-resolved CCN  
96 measurements as well as particle number size distribution (PSD) measurements. The  
97 measured aerosol PSD is within the size range of 14-600 nm. Aerosol chemical  
98 composition was measured simultaneously by an Aerodyne Aerosol Chemical  
99 Speciation Monitor (ACSM) (Sun et al., 2012).

100 The aerosol inlet for the size distribution measurements was equipped with a TSI  
101 Environmental Sampling System (Model 3031200), which consists of a sharp-cut  
102 PM<sub>1</sub> cyclone and a bundled nafion dryer. The size-resolved CCN efficiency spectra  
103 were measured by coupling the DMT-CCN<sub>C</sub> used with the SMPS (Rose et al., 2008).  
104 In this step, the particles are rapidly dried with RH < 30% upon entering the  
105 Differential Mobility Analyzer (DMA). Thus, size selection is effectively performed  
106 under dry conditions. Relative deviations in particle diameter should be < 1% except  
107 for potential kinetic limitations (Mikhailov et al., 2009). The sample flow exiting the

108 DMA was split into two parts: 0.3 lpm for the CPC and 0.5 lpm for the CCN counter  
109 (CCN<sub>C</sub>). The DMA, controlled by TSI-AIM software, scanned one size distribution  
110 every five minutes. The CCN<sub>C</sub> was operated at a total flow rate of 0.5 lpm with a  
111 sheath-to-aerosol flow ratio of 10. The inlet RH for CCN<sub>C</sub> was < 30%. During the  
112 field campaign, the mean sample temperature and pressure measured by CCN<sub>C</sub>  
113 sensors was (24.3±1.4) °C and (898.4±11.7) hPa. The supersaturations levels of CCN<sub>C</sub>  
114 were calibrated with ammonium sulfate before and after the field campaign, following  
115 the procedures outlined in [Rose et al. \(2008\)](#). During each CCN measurement cycle,  
116 calibrated effective supersaturations were set at 0.075%, 0.13%, 0.17%, 0.39%, and  
117 0.75%. The overall error (1σ) for the supersaturation levels was estimated to be <  
118 3.5%. The completion of a full measurement cycle took 50 minutes (10 minutes for  
119 each supersaturation level).

120 The measurement of non-refractory submicron aerosol species including  
121 organics, sulfate, nitrate, ammonium, and chloride were made with an ACSM. During  
122 the field campaign, ambient aerosols were drawn inside through a ½ inch (outer  
123 diameter) stainless steel tube at a flow rate of ~3 L min<sup>-1</sup>, of which ~84 cc min<sup>-1</sup> was  
124 sub-sampled into the ACSM. An URG cyclone (Model: URG-2000-30ED) was also  
125 positioned in front of the sampling inlet to remove coarse particles with a cut-off size  
126 of 2.5 μm. Before sampling into the ACSM, aerosol particles were dried using a silica  
127 gel desiccant. The residence time in the sampling tube was ~5 s. The ACSM was  
128 operated at a time resolution of ~15 min with a scan rate of mass spectrometer at 500  
129 ms amu<sup>-1</sup> from m/z 10 to 150. Regarding the calibration of the ACSM,  
130 mono-dispersed, size-selected 300-nm ammonium nitrate particles within a range of  
131 concentrations were sampled into both the ACSM and a condensation particle counter  
132 (CPC). The ionization efficiency (IE) was then determined by comparing the response



133 factors of the ACSM to the mass calculated with known particle size and number  
134 concentrations from the CPC. More detailed descriptions of the operation and  
135 calibration of the ACSM are given in Sun et al. (2012) and Ng et al. (2011). The  
136 campaign averaged mass concentration of  $PM_{10}$  is  $31.6 \mu\text{g m}^{-3}$ .

137 In addition to the ACSM, the black carbon (BC) in  $PM_{2.5}$  was simultaneously  
138 measured at a time resolution of 5 min by a seven-wavelength aethalometer (Model  
139 AE31, Magee Scientific Corporation). The campaign averaged mass concentration of  
140 BC is  $\sim 2.5 \mu\text{g m}^{-3}$ . During the experiment, the campaign area was generally hot and  
141 dry, with an average temperature of  $21.6 \text{ }^\circ\text{C}$  and an average ambient RH of 69.5%.

## 142 2.2 Data

143 The raw CCN data were first filtered according to instrument recorded  
144 parameters (e.g., temperature and flow). For example, if the relative difference  
145 between the actual and preset sample flows was larger than 4%, the data are flagged  
146 as invalid. The data is also excluded if the “temperature stability” was flagged as “0”.  
147 These flagged data are not used for further analysis. A multiple charge correction and  
148 transfer function (Deng et al., 2011) is applied to each PSD as well as to the CCN  
149 efficiency spectrum. The CCN activation ratio (AR) is the ratio of  $N_{CCN}$  to CN  
150 concentration ( $N_{CN}$ ). Bulk AR is calculated from the total  $N_{CN}$  and  $N_{CCN}$ . For the  
151 size-resolved CCN measurements, we get size-resolved AR from size-resolved CCN  
152 and CN number concentrations.

153 Size-resolved CCN and PSD data, measured with a DMT-CCNc and a SMPS  
154 (with a particle size range of 10-700 nm) on 7-21 July 2013 at Xianghe (Zhang et al.,  
155 2014), are used in this study for comparisons with CCN activity at the Xinzhou site.  
156 Aerosol mass concentrations were processed using the ACSM standard data analysis

157 software (version 1.5.3.0). Detailed procedures for the data analysis have been  
 158 described by Ng et al. (2011) and Sun et al. (2012).

### 159 3. Derivation of $\kappa_{chem}$

160 In this study, we calculate  $\kappa_{chem}$  based on bulk chemical composition observations  
 161 made during the field campaign. The method is very similar to that used by Zhang et  
 162 al., (2014). As proposed by Petters and Kreidenweis (2007),  $\kappa_{chem}$  can be predicted  
 163 using a simple mixing rule based on chemical volume fractions for a given internal  
 164 mixture:

$$165 \quad \kappa_{chem} = \sum_i \varepsilon_i \kappa_i \quad (1)$$

166 where  $\kappa_i$  and  $\varepsilon_i$  are the hygroscopicity parameter and volume fraction, respectively, for  
 167 the individual (dry) components in the mixture and  $i$  is the number of components in  
 168 the mixture.

169 Measurements from the ACSM in Xinzhou show that the composition of  
 170 submicron particles was dominated by organics, followed by sulfate, ammonium, and  
 171 nitrate. The contribution of chloride was negligible (volume fraction of about < 2%).  
 172 The analysis of the anion and cation balance suggests that anionic species ( $\text{NO}_3^-$ ,  
 173  $\text{SO}_4^{2-}$ ) were essentially neutralized by  $\text{NH}_4^+$  over the relevant size range. For  
 174 refractory species, BC represented a negligible fraction of the total submicron aerosol  
 175 volume (< 3%). Sea salt and dust are usually coarse mode particles with particle sizes >  
 176  $1 \mu\text{m}$  (Whitby, 1978). The contribution of such types of aerosols is thus expected to be  
 177 negligible for sizes <  $1 \mu\text{m}$ . Therefore, the submicron particles measured by the ACSM  
 178 mainly consisted of organics,  $(\text{NH}_4)_2\text{SO}_4$ , and  $\text{NH}_4\text{NO}_3$ . The particle hygroscopicity is  
 179 thus the volume average of the three participating species:

$$180 \quad \kappa_{chem} = \kappa_{Org} \varepsilon_{Org} + \kappa_{(\text{NH}_4)_2\text{SO}_4} \varepsilon_{(\text{NH}_4)_2\text{SO}_4} + \kappa_{\text{NH}_4\text{NO}_3} \varepsilon_{\text{NH}_4\text{NO}_3} \quad (2)$$

181 Here, the values of  $\kappa$  for  $(\text{NH}_4)_2\text{SO}_4$  and  $\text{NH}_4\text{NO}_3$  are 0.67 and 0.61, respectively.

182 The following linear function derived by Mei et al. (2013) was used to estimate  $\kappa_{Org}$  in  
183 this study:  $\kappa_{Org} = 2.10 \times f_{44} - 0.11$ , where  $f_{44}$  is the fraction of m/z 44 in total organics.  
184 The mean value of  $\kappa_{Org}$  during the field campaign is  $0.115 \pm 0.019$ .

## 185 4. Results and discussion

### 186 4.1 CCN efficiency spectra

187 During the field campaign at the Xinzhou site, ~790 size-resolved CCN  
188 efficiency spectra at five supersaturation levels ranging from 0.075% to 0.76% were  
189 measured. Figure 1 shows campaign averaged spectra of the measured CCN  
190 efficiency at Xinzhou for supersaturation levels of 0.075%, 0.13%, 0.17%, 0.39%, and  
191 0.76%. The observed averaged CCN efficiency spectra during Xianghe campaign in  
192 summer 2013 are also shown. The right panels show the mass concentration fraction  
193 of particle chemical compositions at Xinzhou (top panel) and Xianghe (bottom panel)  
194 during their respective observation periods. Significant differences in size-resolved  
195 CCN efficiency spectra at the two sites are seen. Aerosol particles at Xinzhou activate  
196 more efficiently (higher values of AR) at a given particle diameter ( $D_p$ ) for the same  
197 supersaturation level. In the other words, a larger  $D_p$  was required to reach the same  
198 activation efficiency at Xianghe. This suggests that aerosol properties at each site  
199 differ.

200 The slope of AR with respect to diameters near  $D_p$  when AR=50% (defined here  
201 as the cut-off diameter,  $D_{cut}$ ) provides information about the heterogeneity of the  
202 composition for size-resolved particles. For an ideal case when all CCN-active  
203 particles have the same composition and size, a steep change in AR from 0 to 1 would  
204 be observed as  $D_p$  reached  $D_{cut}$ . A gradual increase in size-resolved AR with  $D_p$   
205 suggests that aerosol particles have different hygroscopicities. The steeper slopes of

206 AR around  $D_{cut}$  observed at Xinzhou suggest that the particle composition was less  
207 heterogeneous with more hygroscopicity than particles at the Xianghe site. This can  
208 be partially explained by the magnitudes of the mean  $\kappa_{chem}$  at the two sites (0.42 at  
209 Xinzhou and 0.38 at Xianghe). Also, the  $f_{44}$  is greater at Xinzhou than at Xianghe. The  
210  $m/z$  44 signal is mostly due to acids (Takegawa et al., 2007; Duplissy et al., 2011) or  
211 acid-derived species, such as esters.  $f_{44}$  is closely related to the organic oxidation level  
212 (Aiken et al., 2008). Oxidized/aged acids are generally more hygroscopic and easily  
213 activated. Moreover, the primary inorganic particles at the Xinzhou site are sulfates,  
214 with a mass fraction that is two times greater than that measured at Xianghe.  
215 Therefore, particles at the Xinzhou site consist of more hygroscopic sulfate-dominant  
216 inorganics and aged/oxidized secondary organics and can thus be more efficiently  
217 activated at a given  $D_p$ , as shown in Fig. 1.

## 218 4.2 Air mass influences on CCN activity: a case study

219 Because air mass back trajectories combined with ambient air measurements can  
220 be used for analyzing large-scale air pollutant transport and source identification at a  
221 receptor site (Stohl, 1996; Rousseau et al., 2004), in this study, we calculated five-day  
222 (120 hr) back trajectories using the Hybrid Single-Particle Lagrangian Integrated  
223 Trajectory (HYSPLIT) model (Draxler and Hess, 1998) with National Centers for  
224 Environmental Prediction (NCEP) reanalysis data. TrajStat software (Wang et al.,  
225 2009) has been used to calculate trajectories. The arrival height of the trajectories at  
226 the Xinzhou site was at the surface.

227 Three cases were selected to study air mass influences on aerosol activity: (1)  
228 Case 1, 19 August 2014, 19:00-21:00 local time (LT); (2) Case 2, 9 August 2014,  
229 03:00-10:00 LT; and (3) Case 3, 29 July 2014, 00:00-12:00 LT. Each case is

230 associated with a different CCN efficiency spectrum, i.e., top, middle, and bottom  
231 panels of Fig. 2 are for Cases 1, 2, and 3, respectively. Their respective back  
232 trajectories are shown in Fig. 3.

233 In Case 1, air trajectories (red line in Fig. 3) originated from the southwest and  
234 passed through northern Shaanxi Province and northwestern Shanxi Province, then  
235 rounded back to the site from the north/northeast. So, aerosols in this case are closely  
236 associated with air parcels north/northeast of the site. The trajectories were very short,  
237 suggesting that the air flow was slow during the observational period. Under these  
238 circumstances, aerosol loading would be largely impacted by local sources around the  
239 site. A high mass fraction of organics ( $> 60\%$ ) with low  $f_{44}$  ( $\sim 10\%$ ) and  $\kappa_{chem}$  ( $< 0.3$ )  
240 values was measured during the observational period. Furthermore, the PSD showed  
241 one peak mode with  $D_p = 56$  nm and a high  $N_{CN}$  ( $\sim 1.7 \times 10^4$  cm $^{-3}$ ), but low mass  
242 concentration of  $PM_{10}$  ( $28.36$   $\mu\text{g m}^{-3}$ ). This suggests that particles may be composed of  
243 freshly emitted primary aerosols (the biogenic emissions from the plants and trees  
244 around the site). This type of aerosol is usually less hygroscopic with a single peak  
245 mode primarily composed of fine particles (Whitby, 1978; Hussein et al., 2005).  
246 These aerosols cannot activate efficiently. The maximum activation fraction (MAF)  
247 shown in the top right panel of Fig. 2 is less than 0.6 at all supersaturation levels for  
248 particles with  $D_p > 300$  nm, indicating that the particles should be largely externally  
249 mixed aerosols.

250 In Case 2 (blue line in Fig. 3), air parcels moved rapidly from the west to the site.  
251 The site should then be influenced by the large-scale transport of air masses. For this  
252 case, aerosols contain a small amount of organics ( $< 30\%$ ), but have high  $f_{44}$  ( $\sim 14\%$ )  
253 and  $\kappa_{chem}$  values ( $\sim 0.5$ ). The PSD showed a double peak mode with an  $N_{CN}$  of  
254  $\sim 1.3 \times 10^4$  cm $^{-3}$  and a relatively high mass concentration of  $PM_{10}$  ( $81.45$   $\mu\text{g m}^{-3}$ ). The

255 double peak mode suggests that aerosols in this case are a mixture of aerosols from  
256 local sources and from other regions (Whitby, 1978; Dal Maso et al., 2007). Because  
257 aerosols are aged and oxidized during long-distance transport, these particles are  
258 usually composed of secondary organic and inorganic components with more  
259 hygroscopicity (Weber et al., 1999; Verver et al., 2000). These aerosols can activate  
260 efficiently. The MAF is close to 1 and the slopes of AR around  $D_{cut}$  are steep at all  
261 supersaturation levels (middle right panel of Fig. 2). This CCN efficiency spectrum is  
262 similar to the ideal spectrum of pure ammonium sulfate.

263 In Case 3 (green line in Fig. 3), air parcels travelled from the northwest to the  
264 site. Air masses arriving at the site in this case had passed over densely populated  
265 regions with more heavy pollution. A gradual increase in size-resolved AR with  $D_p$  is  
266 seen (bottom right panel of Fig. 2). This is attributed to the diversity in aerosol  
267 hygroscopicity because of the complex nature of the chemical composition of aerosol  
268 particles.

### 269 4.3 Correlation of $N_{CN}$ and $N_{CCN}$

270 Figure 4 shows  $N_{CN}$  as a function of  $N_{CCN}$  for different supersaturation levels at  
271 the Xinzhou and Xianghe sites. They showed high or moderate correlations at high  
272 supersaturation levels (e.g.,  $R^2 = 0.57$  at Xinzhou and  $R^2 = 0.85$  at Xianghe at a  
273 supersaturation level of  $\sim 0.8\%$ ), but quite poor correlations at low supersaturation  
274 levels. Although Andreae (2009) proposed using the relationship of CCN and CN, or  
275 even aerosol optical depth (AOD), to parameterize CCN in models, it should be  
276 caution if one uses the correlation especially for those cases at low supersaturations  
277 because of the spatial variation in CCN activity for maritime and continental aerosols.  
278 It was noticed that there was an apparent higher degree of correlation at Xianghe site

279 for each supersaturation than that derived at Xinzhou site. In view of the similar regimes  
280 from which the data are taken and the same instruments by which they have been collected,  
281 the discrepancy between Xianghe and Xinzhou should be caused largely by the spatial  
282 variations of aerosols types. These variations are primarily attributed to variations in  
283 aerosol particle size, i.e., the shape of the PSD as well as particle composition. As  
284 presented by Zhang et al. (2014), the relationship between bulk activation ratios and  
285  $N_{CCN}$  was complex under polluted conditions and was heavily dependent on the  
286 physicochemical properties of atmospheric aerosols.

#### 287 **4.4 Impact of $x_{org}$ on $N_{CCN}$**

288 Precise quantification of  $N_{CCN}$  is crucial for understanding aerosol indirect  
289 effects and characterizing these effects in models. A CCN closure study is useful to  
290 examine the controlling physical and chemical factors and to help verify experimental  
291 results.  $N_{CCN}$  is usually derived from measured aerosol properties, such as PSD and  
292 composition or hygroscopicity based on the Köhler theory. Achieving such closure  
293 under heavily polluted conditions is more challenging, especially due to the complex  
294 effects of organics on CCN activity. In this section, we examine the sensitivity of  
295 volume fraction of organics ( $x_{org}$ ) as well as oxidation or aging of organics to  $N_{CCN}$   
296 estimation based on measurement at Xinzhou site. During the observed period,  
297 aerosols at the Xinzhou site were dominated by organics, with 12%, 23%, 39%, and 25% of  
298 the data points corresponding to  $x_{org} > 60\%$ ,  $50\% < x_{org} < 60\%$ ,  $40\% < x_{org} < 50\%$  and  $x_{org}$   
299  $< 40\%$ , respectively. For the purpose of examining the sensitivity of estimated  $N_{CCN}$  to  
300  $x_{org}$  and oxidation/aging level, we sorted the size-resolved CCN data when the  
301  $x_{org} > 60\%$ ,  $50\% < x_{org} < 60\%$ ,  $40\% < x_{org} < 50\%$  and  $x_{org} < 40\%$ . Furthermore, for each  
302 level of  $x_{org}$ , we tested the impacts on  $N_{CCN}$  estimation both from the most oxidized  
303 (with  $f_{44}$  of higher than 15%) and least oxidized (those primary organic aerosols with

304  $f_{44}$  of lower than 11%) organic particles. For example, the size-resolved CCN data  
305 points during the period when  $x_{\text{org}} > 60\%$  and also  $f_{44} > 15\%$  was averaged to generate  
306 the averaged CCN efficiency spectra at the five supersaturations respectively. Then  
307 we used the produced averaged CCN efficiency spectra to estimate  $N_{\text{CCN}}$ .

308 Estimated CCN size distributions at the five supersaturations were firstly  
309 calculated by multiplying the averaged CCN efficiency spectrum (by using the  
310 averaged CCN efficiency spectra, the aerosol particles were assumed with uniform  
311 chemical composition without considering the effects of the temporal variations of the  
312 activation curves on CCN activity) with the actually measured PSD. Then, we  
313 integrated the estimated CCN size distribution over the whole size range to generate  
314 estimated  $N_{\text{CCN}}$ . While the measured CCN size distributions are integrated to produce  
315 the observed  $N_{\text{CCN}}$ .

316 Observed and estimated  $N_{\text{CCN}}$  at four supersaturation levels (0.075%, 0.13, 0.17  
317 and 0.76%) were showed in Fig 5. The data points presented more disperse and  
318 weaker correlations at lower supersaturations. The sensitivity of volume fraction of  
319 organics to  $N_{\text{CCN}}$  increased with increasing  $x_{\text{org}}$ . This is especially for the case of these  
320 primary organic particles with  $f_{44} < 11\%$ : the slopes obtained from a linear fit of  
321 estimated and measured  $N_{\text{CCN}}$  in Fig 6 decreased rapidly (almost with a decrease of  
322 ~50%) when the  $x_{\text{org}}$  varied from  $< 40\%$  to  $> 60\%$  at supersaturations of 0.075%, while  
323 it didn't exhibit a lot of reduction (merely ~10%) along with the increasing of  $x_{\text{org}}$  for  
324 the supersaturation of 0.76%.  $N_{\text{CCN}}$  was estimated most accurately at higher  
325 supersaturation levels. This is likely because a large fraction of particles was already  
326 CCN-active. Also, particle composition has relatively less influence on CCN  
327 activation at high supersaturations (Twohy and Anderson, 2008). For the oxidized or  
328 aged particles with  $f_{44} > 15\%$ , the slopes still follow the similar tendency with the



329 variations of  $x_{\text{org}}$  at low and high supersaturations but changed more smoothly to the  
330  $x_{\text{org}}$  attributing to the oxidized/aged organic particles being more hygroscopic.

331 However, the impacts of the aerosol particles oxidization level on estimating  
332  $N_{\text{CCN}}$  were also very significant. For example, when the particles were composed by  
333 large amounts of organics ( $x_{\text{org}} > 60\%$ ), the  $N_{\text{CCN}}$  at the supersaturation of 0.075% and  
334 0.13% was underestimated by 46% and 44% respectively at  $f_{44} < 11\%$ , while the  
335 underestimation decreased to 32% and 23% at the corresponding supersaturation level  
336 at  $f_{44} > 15\%$ . The  $N_{\text{CCN}}$  at  $ss = 0.76$  was underestimated by 11% and 4% respectively at  
337  $f_{44} < 11\%$  and  $f_{44} > 15\%$ . One thus could conclude that the estimation of  $N_{\text{CCN}}$  would be  
338 largely improved if the aerosol particles were aged with high oxidation level,  
339 especially when the chemical composition of the particles is dominated by organics.  
340 But for the particles with relative low organics ( $x_{\text{org}} < 40\%$ ), the effect caused by the  $f_{44}$   
341 was quite insignificant both for high and low supersaturations. In Fig 6, the slopes  
342 were all around 1.0 at the two cases of  $f_{44} < 11\%$  and  $f_{44} > 15\%$ . This can be easily  
343 explained. When  $x_{\text{org}}$  is less than 40%, the overall hygroscopicity of the particles is  
344 dominated by inorganic species such as sulfate and nitrate, which are more  
345 hygroscopic ( $\kappa_{\text{inorg}}$  usually larger than 0.6) than organic compounds ( $\kappa_{\text{org}}$  usually smaller  
346 than 0.2). As a result, a larger fraction of particles can be activated. According to the  
347 simple mixing rule based on chemical volume fractions proposed by [Petters and](#)  
348 [Kreidenweis \(2007\)](#), the contribution from organics is quite small. If  $x_{\text{org}}$  is greater  
349 than 60%, organics will dominate the overall particle hygroscopicity. Particles with a  
350 large  $f_{44}$  are much more hygroscopic and thus strongly influence the estimated  $N_{\text{CCN}}$ .  
351 Our results indicated that increasing the proportion of secondary organics would  
352 decrease the uncertainties in estimating  $N_{\text{CCN}}$  and lead to a more accurate estimation  
353 of  $N_{\text{CCN}}$ .

#### 354 4.5 Applicability of CCN efficiency spectra

355 As a means of testing the applicability of the CCN activation spectra, campaign  
356 mean CCN efficiency spectra at different supersaturations observed at the Xinzhou  
357 site is used to estimate  $N_{\text{CCN}}$  at the Xinzhou and Xianghe sites respectively, which  
358 helps to further examine the sensitivity of  $N_{\text{CCN}}$  to aerosol type. Data from the two  
359 sites were measured during the warm season so that the effect of temporal variations  
360 in aerosols on CCN levels is reduced. Fitted campaign mean CCN efficiency spectrum  
361 at the five supersaturations at Xinzhou (corresponding to spectra in Fig. 1) is  
362 multiplied by dry PSDs actually measured at Xinzhou and at the Xianghe site  
363 respectively. This generates estimated CCN size distributions at the two sites. They  
364 are then integrated over the whole size range (14-600 nm and 10-700 nm at the  
365 Xinzhou and Xianghe sites, respectively) to obtain the estimated  $N_{\text{CCN}}$ . The measured  
366 CCN size distributions at each site are integrated to produce the observed  $N_{\text{CCN}}$ .

367 Figure 7 shows estimated  $N_{\text{CCN}}$  as a function of measured  $N_{\text{CCN}}$  for different  
368 supersaturation levels at the two sites.  $N_{\text{CCN}}$  at Xinzhou was underestimated by 4-5%  
369 at supersaturation levels of 0.39% and 0.76%, and was slightly overestimated (~2%)  
370 at Xianghe for the same supersaturation levels. Good agreement is seen at the 0.39%  
371 and 0.76% supersaturation levels for data from both sites ( $R^2 > 0.92$ ).  $N_{\text{CCN}}$  at  
372 Xinzhou was underestimated by ~7% at supersaturation levels  $< 0.1\%$  ( $R^2 = 0.87$ ). At  
373 Xianghe, however,  $N_{\text{CCN}}$  was overestimated by 19-23% at supersaturation levels  $< 0.1\%$   
374 although the correlation between calculated and measured  $N_{\text{CCN}}$  was good. Because  
375 size-resolved CCN efficiency spectra were applied here, excluding the impact of  
376 particle size, the influence of chemical composition on CCN activation can be  
377 investigated. The poor estimates of CCN at low supersaturation levels could be  
378 attributed to the high sensitivity of  $N_{\text{CCN}}$  to chemical composition. Because the mass

379 fractions of inorganics and organics measured at the two sites are similar (Fig. 1) and  
380 the hygroscopicity for inorganic components is fixed, this overestimation is attributed  
381 to the smaller proportion of aged and oxidized organic aerosols at Xianghe compared  
382 with aerosols at Xinzhou ( $f_{44} = 17\%$  and  $11\%$  at Xinzhou and Xianghe, respectively).

## 383 5. Summary and conclusions

384 In this study, we have investigated the impacts of particle physicochemical  
385 properties on CCN activity based on field measurements obtained from 22 July to 26  
386 August of 2014 in the suburb of Xinzhou, China. Five-day back trajectories combined  
387 with measurements were analyzed to examine air mass influences on CCN activity.  
388 CCN efficiency was largely reduced by local primary biomass burning events, and the  
389 MAF was low to  $<60\%$ , suggesting externally-mixed and the heterogeneity of particle  
390 composition for local emitted aerosols. The CCN activation efficiency was enhanced  
391 significantly when the site was under the influence of air transported from far away,  
392 during which aerosols could be mixed well with more hygroscopic secondary organic  
393 and inorganic components. The relationship between  $N_{CN}$  and  $N_{CCN}$  was generally  
394 poor. Large errors would arise if using the former to estimate the latter, especially  
395 under low supersaturation conditions.

396 The sensitivity of  $x_{org}$  as well as  $f_{44}$  on estimating  $N_{CCN}$  has also been examined.  
397 A strong dependence of  $N_{CCN}$  on the both two parameters was noted. The sensitivity  
398 of volume fraction and particles oxidization or aging level of organics to  $N_{CCN}$   
399 increased with increasing  $x_{org}$ . And also this dependence weakens as the  
400 supersaturation level increases. When the particles were mostly composed of organics  
401 ( $x_{org} > 60\%$ ), the  $N_{CCN}$  at the supersaturation of  $0.075\%$  and  $0.13\%$  was underestimated  
402 by  $46\%$  and  $44\%$  respectively if aerosol particles were freshly emitted with primary  
403 organics ( $f_{44} < 11\%$ ); while the underestimation decreased to  $32\%$  and  $23\%$  at the

404 corresponding supersaturations if the particles were with more hygroscopic secondary  
405 organics( $f_{44}>15\%$ ). The  $N_{CCN}$  at the supersaturation of 0.76% was underestimated by  
406 11% and 4% respectively at  $f_{44}<11\%$  and  $f_{44}>15\%$ . But for the particles composed of  
407 low organics (e.g.  $x_{org}<40\%$ ), the effect caused by the  $f_{44}$  was quite insignificant both  
408 at high and low supersaturations. This is due to that the overall hygroscopicity of the  
409 particles is dominated by inorganics such as sulfate and nitrate, which are more  
410 hygroscopic than organic compounds. Our results indicated that it would decrease the  
411 uncertainties in estimating  $N_{CCN}$  and lead to a more accurate estimation of  $N_{CCN}$  to  
412 increase the proportion of secondary organics, especially when the composition of the  
413 aerosols is dominated by organics.

414 The applicability of the CCN efficiency spectrum measured at the Xinzhou site  
415 to the Xianghe site was examined and a good agreement was found when the  
416 supersaturation level was  $> 0.2\%$ . However,  $N_{CCN}$  at the Xianghe site was  
417 overestimated by 19-23% when the supersaturation level was  $< 0.1\%$ . Because of the  
418 similar mass fractions of inorganics and organics measured at the two sites, we  
419 conclude that this overestimation was mainly caused by the smaller proportion of  
420 aged and oxidized organic aerosols at Xianghe compared with aerosols at Xinzhou.

## 421 **Acknowledgements**

422 This work was funded by the National Basic Research Program of China '973' (Grant  
423 No. 2013CB955801, 2013CB955804), the Fundamental Research Funds for the  
424 Central Universities (Grant No. 2013YB35) and the NSCF-TAMU Collaborative  
425 Research Grant Program (Grant No. 4141101031). We also acknowledge the members  
426 of the A<sup>2</sup>C<sup>2</sup> team for their hard work during the campaign, including Mr. Du Wei  
427 (from the State Key Laboratory of Atmospheric Boundary Layer Physics and  
428 Atmospheric Chemistry of the Institute of Atmospheric Physics/Chinese Academy of

429 Sciences for carrying out the chemical composition measurements) and Mr. Yuan  
430 Cheng (from Nanjing University who helped make the size-resolved CCNc  
431 measurements).

## 432 **References**

433 Aiken, A. C., DeCarlo, P. F., Kroll, J. H., Worsnop, D. R., Huffman, J. A., Docherty,  
434 K. S., Ulbrich, I. M., Mohr, C., Kimmel, J. R., Sueper, D., Sun, Y., Zhang, Q.,  
435 Trimborn, A., Northway, M., Ziemann, P. J., Canagaratna, M. R., Onasch, T. B.,  
436 Alfarra, M. R., Prevot, A. S. H., Dommen, J., Duplissy, J., Metzger, A.,  
437 Baltensperger, U., and Jimenez, J. L.: O/C and OM/OC ratios of primary,  
438 secondary, and ambient organic aerosols with high-resolution time-of-flight aerosol  
439 mass spectrometry, *Environ. Sci. Technol.*, 42, 4478–4485, 2008.

440 Andreae, M.O.: Correlation between cloud condensation nuclei concentration and  
441 aerosol optical thickness in remote and polluted regions, *Atmos. Chem. Phys.*, 9,  
442 543-556, 2009.

443 Bougiatioti, A., Fountoukis, C., Kalivitis, N., Pandis, S. N., Nenes, A., and  
444 Mihalopoulos, N.: Cloud condensation nuclei measurements in the marine  
445 boundary layer of the eastern Mediterranean: CCN closure and droplet growth  
446 kinetics. *Atmos. Chem. Phys.*, 9, 7053–7066, 2009.

447 Bougiatioti, A., Nenes, A., Fountoukis, C., Kalivitis, N., Pandis, S. N., and  
448 Mihalopoulos, N.: Size-resolved CCN distributions and activation kinetics of aged  
449 continental and marine aerosol, *Atmos. Chem. Phys.*, 11, 8791-8808,  
450 doi:10.5194/acp-11-8791-2011, 2011.

451 Chuang, P. Y., Collins, D. R., Pawlowska, H., Snider, J. R., Jonsson, H. H., Brenguier,  
452 J. L., Flagan, R. C., and Seinfeld, J. H.: CCN measurements during ACE-2 and  
453 their relationship to cloud microphysical properties, *Tellus B*, 52, 843–867, 2000.

- 454 Clarke, A., McNaughton, C., Kasputin, V. N., Shinozuka, Y., Howell, S., Dibb, J.,  
455 Zhou, J., Anderson, B., Brekhovskikh, V., Turner, H., and Pinkerton, M.: Biomass  
456 burning and pollution aerosol over North America: Organic components and their  
457 influence on spectral optical properties and humidification response, *J. Geophys.*  
458 *Res.*, 112, D12S18, doi:10.1029/2006JD007777, 2007.
- 459 Dal Maso, M., L. Sogacheva, P. P. Aalto, I. Riipinen, M. Komppula, P. Tunved, L.  
460 Korhonen, V. SUUR@USKI, A. Hirsikko, and T. KurtEN, Aerosol size  
461 distribution measurements at four Nordic field stations: identification, analysis  
462 and trajectory analysis of new particle formation bursts, *Tellus B*, 2007, 59(3),  
463 350-361.
- 464 Deng, Z., Zhao, C., Ma, N., Liu, F., Ran, L., Xu, W., Liang, Z., Liang, S., Huang, M.,  
465 Ma, X., Zhang, Q., Quan, J., and Yan, P.: Size- resolved and bulk activation  
466 properties of aerosols in the North China Plain. *Atmos. Chem. Phys.*, 11,  
467 3835-3846, 2011.
- 468 Deng, Z., Zhao, C., Ma, N., Ran, L., Zhou, G., Lu, D., and Zhou, X.: An examination  
469 of parameterizations for the CCN number concentration based on in situ  
470 measurements of aerosol activation properties in the North China Plain, *Atmos.*  
471 *Chem. Phys.*, 13, 6227–6237, doi:10.5194/acp-13-6227-2013, 2013.
- 472 Draxler, R., R. and Hess, G., D. 1998. An overview of the HYSPLIT 4 modeling  
473 system for trajectories, dispersion, and deposition, *Aust. Meteorol. Mag.* 47, 295–  
474 308.
- 475 Duplissy, J., DeCarlo, P. F., Dommen, J., Alfarra, M. R., Metzger, A., Barmpadimos,  
476 I., Prevot, A. S. H., Weingartner, E., Tritscher, T., Gysel, M., Aiken, A. C., Jimenez,  
477 J. L., Canagaratna, M. R., Worsnop, D. R., Collins, D. R., Tomlinson, J., and  
478 Baltensperger, U.: Relating hygroscopicity and composition of organic aerosol

- 479 particulate matter, *Atmos. Chem. Phys.*, 11, 1155–1165,  
480 doi:10.5194/acp-11-1155-2011, 2011.
- 481 Dusek, U., Covert, D. S., Wiedensohler, A., Neususs, C., Weise, D., and Cantrell, W.:  
482 Cloud condensation nuclei spectra derived from size distributions and hygroscopic  
483 properties of the aerosol in coastal south-west Portugal during ACE-2, *Tellus B*, 55,  
484 35–53, 2003.
- 485 Engelhart, G. J., Hennigan, C. J., Miracolo, M. A., Robinson, A. L., and Pandis, S. N.:  
486 Cloud condensation nuclei activity of fresh primary and aged biomass burning  
487 aerosol, *Atmos. Chem. Phys.*, 12, 7285–7293, doi:10.5194/acp-12-7285-2012,  
488 2012.
- 489 Ervens, B., Cubison, M. J., Andrews, E., Feingold, G., Ogren, J.A., Jimenez, J. L.,  
490 Quinn, P. K., Bates, T. S., Wang, J., Zhang, Q., Coe, H., Flynn, M., and Allan, J. D.:  
491 CCN predictions using simplified assumptions of organic aerosol composition and  
492 mixing state: a synthesis from six different locations, *Atmos. Chem. Phys.*, 10,  
493 4795–4807, doi:10.5194/acp-10-4795-2010, 2010.
- 494 Gasparini, R., Collins, D. R., Andrews, E., Sheridan, P. J., Ogren, J. A., and Hudson, J.  
495 G.: Coupling aerosol size distributions and size-resolved hygroscopicity to predict  
496 humidity-dependent optical properties and cloud condensation nuclei spectra., *J.*  
497 *Geophys. Res.*, 111, D05S13, doi:10.1029/2005JD006092, 2006.
- 498 Gunthe SS; Rose D; Su H; Garland RM; Achtert P; Nowak A; Wiedensohler A;  
499 Kuwata M; Takegawa N; Kondo Y; Hu M; Shao M; Zhu T; Andreae MO; Pöschl  
500 U (2011) Cloud condensation nuclei (CCN) from fresh and aged air pollution in  
501 the megacity region of Beijing, *Atmospheric Chemistry and Physics*, 11,  
502 pp.11023-11039. doi: 10.5194/acp-11-11023-2011
- 503 Guo, S., Hu, M., Zamora, M. L., Peng, J., Shang, D., Zheng, J., Zhuofei Du, Zhijun

- 504 Wu, Min Shao, Limin Zeng, Mario J. Molina,<sup>1</sup> and Zhang, R. (2014).  
505 Elucidating severe urban haze formation in China. Proceedings of the National  
506 Academy of Sciences of the United States of America, 111(49), 17373–17378.  
507 doi:10.1073/pnas.1419604111
- 508 Hartz, K. E. H., Tischuk, J. E., Chan, M. N., Chan, C. K., Donahue, N. M., and Pandis,  
509 S. N.: Cloud condensation nuclei activation of limited solubility organic aerosol,  
510 Atmos. Environ., 40, 605–617, 2006.
- 511 Hings, S. S., Wrobel, W. C., Cross, E. S., Worsnop, D. R., Davidovits, P., and Onasch,  
512 T. B.: CCN activation experiments with adipic acid: effect of particle phase and  
513 adipic acid coatings on soluble and insoluble particles, Atmos. Chem. Phys., 8,  
514 3735–3748, doi:10.5194/acp-8-3735-2008, 2008.
- 515 Hudson, J. G. and Da, X. Y.: Volatility and size of cloud condensation nuclei, J.  
516 Geophys. Res., 101, 4435–4442, 1996.
- 517 Hussein, T., M. Dal Maso, T. PETÄJÄ, I. K. KOPONEN, P. PAATERO, P. P.  
518 AALTO, K. HÄMERI, and M. KULMALA, Evaluation of an automatic  
519 algorithm for fitting the particle number size distributions, BOREAL  
520 ENVIRONMENT RESEARCH, 2005, 10(5), 337-355.
- 521 Junge, C. and McLaren, E.: Relationship of cloud nuclei spectra to aerosol size  
522 distribution and composition, J. Atmos. Sci., 28, 382–390, 1971.
- 523 Kammermann, L., Gysel, M., Weingartner, E., Herich, H., Cziczo, D. J., Holst, T.,  
524 Svenningsson, B., Arneth, A., and Baltensperger, U.: Subarctic atmospheric aerosol  
525 composition: 3. Measured and modeled properties of cloud condensation nuclei, J.  
526 Geophys. Res., 115, D04202, doi:10.1029/2009JD012447, 2010.
- 527 Köhler, H.: The nucleus in and growth of hygroscopic droplets, Trans. Faraday Soc.,  
528 32, 1152–1161, doi:10.1039/TF9363201152, 1936.



- 529 Lance, S., Medina, J., Smith, J., and Nenes, A.: Mapping the operation of the DMT  
 530 continuous flow CCN counter, *Aerosol Sci. Technol.*, 40 , 242–254, 2006.
- 531 Lathem, T. L., Beyersdorf, A. J., Thornhill, K. L., Winstead, E. L., Cubison, M. J.,  
 532 Hecobian, A., Jimenez, J. L., Weber, R. J., Anderson, B. E., and Nenes, A.: Analysis  
 533 of CCN activity of Arctic aerosol and Canadian biomass burning during summer  
 534 2008, *Atmos. Chem. Phys.*, 13, 2735-2756, doi:10.5194/acp-13-2735-2013, 2013.
- 535 Lee, Y. S., Collins, D. R., Li, R. J., Bowman, K. P., and Feingold, G.: Expected  
 536 impact of an aged biomass burning aerosol on cloud condensation nuclei and cloud  
 537 droplet concentrations, *J. Geophys. Res.*, 111, D22204, doi:10.1029/2005JD006464,  
 538 2006.
- 539 Li, Z., Chen, H., Cribb, M., Dickerson, R. E., Holben, B., Li, C., Lu, D., Luo, Y.,  
 540 Maring, H., Shi, G., Tsay, S.-C., Wang, P., Wang, Y., Xia, X., Zheng, Y., Yuan, T.,  
 541 and Zhao, F.: Preface to special section on East Asian Studies of Tropospheric  
 542 Aerosols: An International Regional Experiment (EASTAIRE), *J. Geophys. Res.*,  
 543 112, D22S00, doi:10.1029/2007JD008853, 2007.
- 544 Li, Z., Li, C., Chen, H., Tsay, S.-C., Holben, B., Huang, J., Li, B., Maring, H., Qian,  
 545 Y., Shi, G., Xia, X., Yin, Y., Zheng, Y., and Zhuang, G.: East Asian Studies of  
 546 Tropospheric Aerosols and Impact on Regional Climate (EAST - AIRC): An  
 547 overview, *J. Geophys. Res.*, 116, D00K34, doi:10.1029/2010JD015257, 2011.
- 548 Liu, X. and Wang, J.: How important is organic aerosol hygroscopicity to aerosol  
 549 indirect forcing? *Environ. Res. Lett.*, 5, 044010,  
 550 doi:10.1088/1748-9326/5/4/044010, 2010.
- 551 McFiggans, G., Artaxo, P., Baltensperger, U., Coe, H., Facchini, M. C., Feingold, G.,  
 552 Fuzzi, S., Gysel, M., Laaksonen, A., Lohmann, U., Mentel, T. F., Murphy, D. M.,  
 553 O’Dowd, C. D., Snider, J. R., and Weingartner, E.: The effect of physical and

- 554 chemical aerosol properties on warm cloud droplet activation, *Atmos. Chem. Phys.*,  
555 6, 2593–2649, doi:10.5194/acp-6-2593-2006, 2006.
- 556 Mei, F., Hayes, P. L., Ortega, A. M., Taylor, J. W., Allan, J. D., Gilman, J. B., Kuster,  
557 W. C., de Gouw, J. A., Jimenez, J. L., and Wang, J.: Droplet activation properties  
558 of organic aerosols observed at an urban site during CalNex-LA, *J. Geophys. Res.*,  
559 118(7), 2903-2917, doi: 10.1002/jgrd.50285, 2013b.
- 560 Mei, F., Setyan, A., Zhang, Q., and Wang, J.: CCN activity of organic aerosols  
561 observed downwind of urban emissions during CARES, *Atmos. Chem. Phys.*, 13,  
562 12155–12169, doi:10.5194/acp-13-12155-2013, 2013a.
- 563 Mikhailov, E., Vlasenko, S., Martin, S. T., Koop, T., and Pöschl, U.: Amorphous  
564 and crystalline aerosol particles interacting with water vapor: conceptual  
565 framework and experimental evidence for restructuring, phase transitions and  
566 kinetic limitations, *Atmos. Chem. Phys.*, 9, 9491–9522,  
567 doi:10.5194/acp-9-9491-2009, 2009.
- 568 Mircea, M., Facchini, M. C., Decesari, S., Cavalli, F., Emblico, L., Fuzzi, S., Vestin,  
569 A., Rissler, J., Swietlicki, E., Frank, G., Andreae, M. O., Maenhaut, W., Rudich, Y.,  
570 and Artaxo, P.: Importance of the organic aerosol fraction for modeling aerosol  
571 hygroscopic growth and activation: a case study in the Amazon Basin, *Atmos.*  
572 *Chem. Phys.*, 5, 3111–3126, 2005, <http://www.atmos-chem-phys.net/5/3111/2005/>.
- 573 Ng, N. L., Herndon, S. C., Trimborn, A., Canagaratna, M. R., Croteau, P. L., Onasch,  
574 T. B., Sueper, D., Worsnop, D. R., Zhang, Q., Sun, Y. L., and Jayne, J. T.: An  
575 Aerosol Chemical Speciation Monitor (ACSM) for Routine Monitoring of the  
576 Composition and Mass Concentrations of Ambient Aerosol, *Aerosol Sci. Tech.*, 45,  
577 770–784, 2011.
- 578 Paramonov, M., Aalto, P. P., Asmi, A., Prisle, N., Kerminen, V.-M., Kulmala, M., and

- 579 Petäjä T.: The analysis of size-segregated cloud condensation nuclei counter  
580 (CCNC) data and its implications for aerosol-cloud interactions, *Atmos. Chem.*  
581 *Phys. Discuss.*, 13, 9681-9731, doi:10.5194/acpd-13-9681-2013, 2013.
- 582 Petters, M. D., and Kreidenweis, S. M.: A single parameter representation of  
583 hygroscopic growth and cloud condensation nucleus activity, *Atmos. Chem. Phys.*,  
584 7, 1961–1971, doi:10.5194/acp-7-1961-2007, 2007.
- 585 Petters, M. D. and Kreidenweis, S. M.: A single parameter representation of  
586 hygroscopic growth and cloud condensation nucleus activity – Part 2: Including  
587 solubility, *Atmos. Chem. Phys.*, 8, 6273–6279, doi:10.5194/acp-8-6273-2008,  
588 2008.
- 589 Raymond, T. M., and Pandis, S. N.: Cloud activation of single component organic  
590 aerosol particles, *J. Geophys. Res.*, 107, 4787, doi:10.1029/2002JD002159, 2002.
- 591 Reutter, P., Su, H., Trentmann, J., Simmel, M., Rose, D., Gunthe, S. S., Wernli, H.,  
592 Andreae, M. O., and Pöschl, U.: Aerosol- and updraft-limited regimes of cloud  
593 droplet formation: influence of particle number, size and hygroscopicity on the  
594 activation of cloud condensation nuclei (CCN), *Atmos. Chem. Phys.*, 9, 7067–7080,  
595 doi:10.5194/acp-9-7067-2009, 2009.
- 596 Rissler, J., Swietlicki, E., Zhou, J., Roberts, G., Andreae, M. O., Gatti, L. V., and  
597 Artaxo, P.: Physical properties of the submicrometer aerosol over the Amazon rain  
598 forest during the wet to dry season transition – comparison of modeled and  
599 measured CCN concentrations, *Atmos. Chem. Phys.*, 4, 2119–2143,  
600 <http://www.atmos-chem-phys.net/4/2119/2004/>, 2004.
- 601 Rissler, J., Vestin, A., Swietlicki, E., Fisch, G., Zhou, J., Artaxo, P., and Andreae, M.  
602 O.: Size distribution and hygroscopic properties of aerosol particles from  
603 dry-season biomass burning in Amazonia, *Atmos. Chem. Phys.*, 6, 471–491,

- 604 doi:10.5194/acp-6-471-2006, 2006.
- 605 Rose, D., Gunthe, S. S., Mikhailov, E., Frank, G. P., Dusek, U., Andreae, M. O., and  
606 Poschl, U.: Calibration and measurement uncertainties of a continuous-flow cloud  
607 condensation nuclei counter (DMT-CCNC): CCN activation of ammonium sulfate  
608 and sodium chloride aerosol particles in theory and experiment, *Atmos. Chem.*  
609 *Phys.*, 8, 1153–1179, 2008, <http://www.atmos-chem-phys.net/8/1153/2008/>.
- 610 Rose, D., Nowak, A., Achtert, P., Wiedensohler, A., Hu, M., Shao, M., Zhang, Y.,  
611 Andreae, M. O., and Poschl, U.: Cloud condensation nuclei in polluted air and  
612 biomass burning smoke near the mega-city Guangzhou, China – Part 1:  
613 Size-resolved measurements and implications for the modeling of aerosol particle  
614 hygroscopicity and CCN activity, *Atmos. Chem. Phys.*, 10, 3365–3383,  
615 doi:10.5194/acp-10-3365-2010, 2010.
- 616 Rousseau, D., D., Duzer, D., Etienne, J., L., Cambon, G., Jolly, D. And coauthors.  
617 2004. Pollen record of rapidly changing air trajectories to the North Pole, *J.*  
618 *Geophys. Res.* 109, D06116, doi:10.1029/2003JD003985.
- 619 Snider, J.R., Guibert, S., Brenguierand, J. L. and Putaud, J. P.: Aerosol activation in  
620 marine stratocumulus clouds: Part – II Köhler and parcel theory closure studies, *J.*  
621 *Geophys. Res.*, 108, doi:10.1029/2002JD002692, 2003
- 622 Sotiropoulou, R. E. P., Nenes, A., Adams, P. J., and Seinfeld, J. H.: Cloud  
623 condensation nuclei prediction error from application of Köhler theory:  
624 Importance for the aerosol indirect effect, *J. Geophys. Res.*, 112, D12202,  
625 doi:10.1029/2006JD007834, 2007.
- 626 Stohl, A. 1996, Trajectory statistics - a new method to establish source-receptor  
627 relationships of air pollutants and its application to the transport of particulate  
628 sulfate in Europe, *Atmos. Environ.* 30, 579–587.

- 629 Stroud, C. A., Nenes, A., Jimenez, J. L., DeCarlo, P., Huffman, J. A., Bruintjes, R.,  
630 Nemitz, E., Delia, A. E., Toohey, D. W., Guenther, A. B., and Nandi, S.: Cloud  
631 Activating Properties of Aerosol Observed during CELTIC, *J. Atmos. Sci.*, 64, 441–  
632 459, 2007.
- 633 Sun, Y., Wang, Z., Dong, H., Yang, T., Li, J., Pan, X., Chen, P., and Jayne, J. T.:  
634 Characterization of summer organic and inorganic aerosols in Beijing, China with  
635 an Aerosol Chemical Speciation Monitor, *Atmos. Environ.*, 51, 250–259,  
636 doi:10.1016/j.atmosenv.2012.01.013, 2012.
- 637 Takegawa, N., Miyakawa, T., Kawamura, K., and Kondo, Y.: Contribution of selected  
638 di-carboxylic and omega-oxocarboxylic acids in ambient aerosol to the m/z 44  
639 signal of an aerodyne aerosol mass spectrometer, *Aerosol Sci. Technol.*, 41, 418–  
640 437, doi:10.1080/02786820701203215, 2007.
- 641 Twohy, C. H. and Anderson, J. R.: Droplet nuclei in non-precipitating clouds:  
642 composition and size matter, *Environ. Res. Lett.*, 3, 045002,  
643 doi:10.1088/1748-9326/3/4/045002, 2008.
- 644 VanReken, T. M., Rissman, T. A., Roberts, G. C., Varutbangkul, V., Jonsson, H. H.,  
645 Flagan, R. C., and Seinfeld, J. H.: Toward aerosol/cloud condensation nuclei (CCN)  
646 closure during CRYSTAL-FACE, *J. Geophys. Res.*, 108, 4633,  
647 doi:10.1029/2003JD003582, 2003.
- 648 VanReken, T. M., Ng, N. L., Flagan, R. C., and Seinfeld, J. H.: Cloud condensation  
649 nucleus activation properties of biogenic secondary organic aerosol, *J. Geophys.*  
650 *Res.*, 110, D07206, doi:10.1029/2004JD005465, 2005.
- 651 Varutbangkul, V., Brechtel, F. J., Bahreini, R., Ng, N. L., Keywood, M. D., Kroll, J.  
652 H., Flagan, R. C., Seinfeld, J. H., Lee, A., and Goldstein, A. H.: Hygroscopicity of  
653 secondary organic aerosols formed by oxidation of cycloalkenes, monoterpenes,

- 654 sesquiterpenes, and related compounds, *Atmos. Chem. Phys.*, 6, 2367–2388, 2006.
- 655 Verver, G., F. Raes, D. Vogelezang, and D. Johnson, The 2nd Aerosol characterization  
656 Experiment (ACE-2): meteorological and chemical context, *Tellus B*, 2000, 52(2),  
657 126-140.
- 658 Wang, J., Lee, Y.-N., Daum, P. H., Jayne, J., and Alexander, M. L.: Effects of aerosol  
659 organics on cloud condensation nucleus (CCN) concentration and first indirect  
660 aerosol effect, *Atmos. Chem. Phys.*, 8, 6325–6339, doi:10.5194/acp-8-6325-2008,  
661 2008.
- 662 Wang, Y.Q., Zhang, X.Y. and Draxler, R., 2009. TrajStat: GIS-based software that  
663 uses various trajectory statistical analysis methods to identify potential sources  
664 from long-term air pollution measurement data. *Environmental Modelling &*  
665 *Software*, 24: 938-939
- 666 Ward, D. S., Eidhammer, T., Cotton, W. R., and Kreidenweis, S. M.: The role of the  
667 particle size distribution in assessing aerosol composition effects on simulated  
668 droplet activation, *Atmos. Chem. Phys.*, 10, 5435–5447,  
669 doi:10.5194/acp-10-5435-2010, 2010.
- 670 Weber, R., P. H. McMurry, R. Mauldin, D. Tanner, F. Eisele, A. Clarke, and V.  
671 Kapustin, New particle formation in the remote troposphere: A comparison of  
672 observations at various sites, *Geophysical Research Letters*, 1999, 26(3),  
673 307-310.
- 674 Wex, H., Hennig, T., Salma, I., Ocskay, R., Kiselev, A., Henning, S., Massling, A.,  
675 Wiedensohler, A., and Stratmann, F.: Hygroscopic growth and measured and  
676 modeled critical super-saturations of an atmospheric HULIS sample, *Geophys. Res.*  
677 *Lett.*, 34, L02818, doi:10.1029/2006GL028260, 2007.
- 678 Whitby, K., T.: The physical characteristics of sulfur aerosols. *Atmos. Environ.*, 12,

679 135-159, 1967, Online publication date: 1-Jan-1978, 1978.

680 Wiedensohler A; Cheng YF; Nowak A; Wehner B; Achtert P; Berghof M; Birmili W;  
681 Wu ZJ; Hu M; Zhu T; Takegawa N; Kita K; Kondo Y; Lou SR; Hofeumahaus A;  
682 Holland F; Wahner A; Gunthe SS; Rose D; Su H; Pöschl U (2009) Rapid aerosol  
683 particle growth and increase of cloud condensation nucleus activity by secondary  
684 aerosol formation and condensation: A case study for regional air pollution in  
685 northeastern China, *Journal of Geophysical Research: Atmospheres*, 114, . doi:  
686 [10.1029/2008JD010884](https://doi.org/10.1029/2008JD010884)

687 Yue, D. L., Hu, M., Zhang, R. J., Wu, Z. J., Su, H., Wang, Z. B., Peng, J. F., He, L.Y.,  
688 Huang, X. F., Gong, Y. G., and Wiedensohler, A.: Potential contribution of new  
689 particle formation to cloud condensation nuclei in Beijing, *Atmos. Environ.*, 45,  
690 6070-6077, 2011.

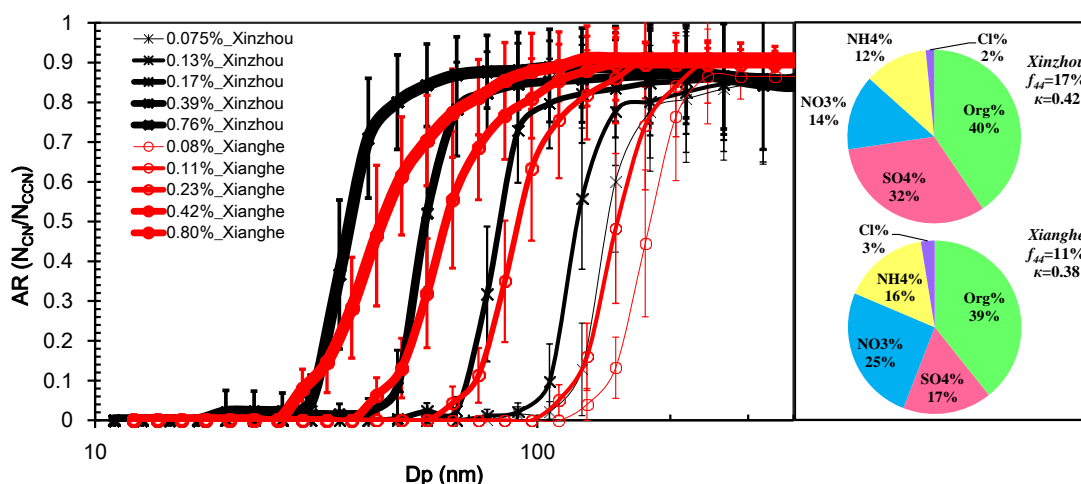
691 Zhang, Q., Meng, J., Quan, J., Gao, Y., Zhao, D., Chen, P., and He, H.: Impact of  
692 aerosol composition on cloud condensation nuclei activity, *Atmos. Chem. Phys.*, 12,  
693 3783-3790, doi:10.5194/acp-12-3783-2012, 2012.

694 Zhang, F., Z. Li, R. J. Li, L. Sun, C. Zhao, P. C. Wang, Y. L. Sun, Y. N. Li, X. G. Liu,  
695 J. X. Li, P. R. Li, G. Ren, and T. Y. Fan., Aerosol hygroscopicity and cloud  
696 condensation nuclei activity during the AC3Exp campaign: implications for cloud  
697 condensation nuclei parameterization. *Atmos. Chem. Phys.*, 14, 13423–13437,  
698 2014

699  
700  
701  
702  
703  
704  
705

706  
707  
708  
709  
710

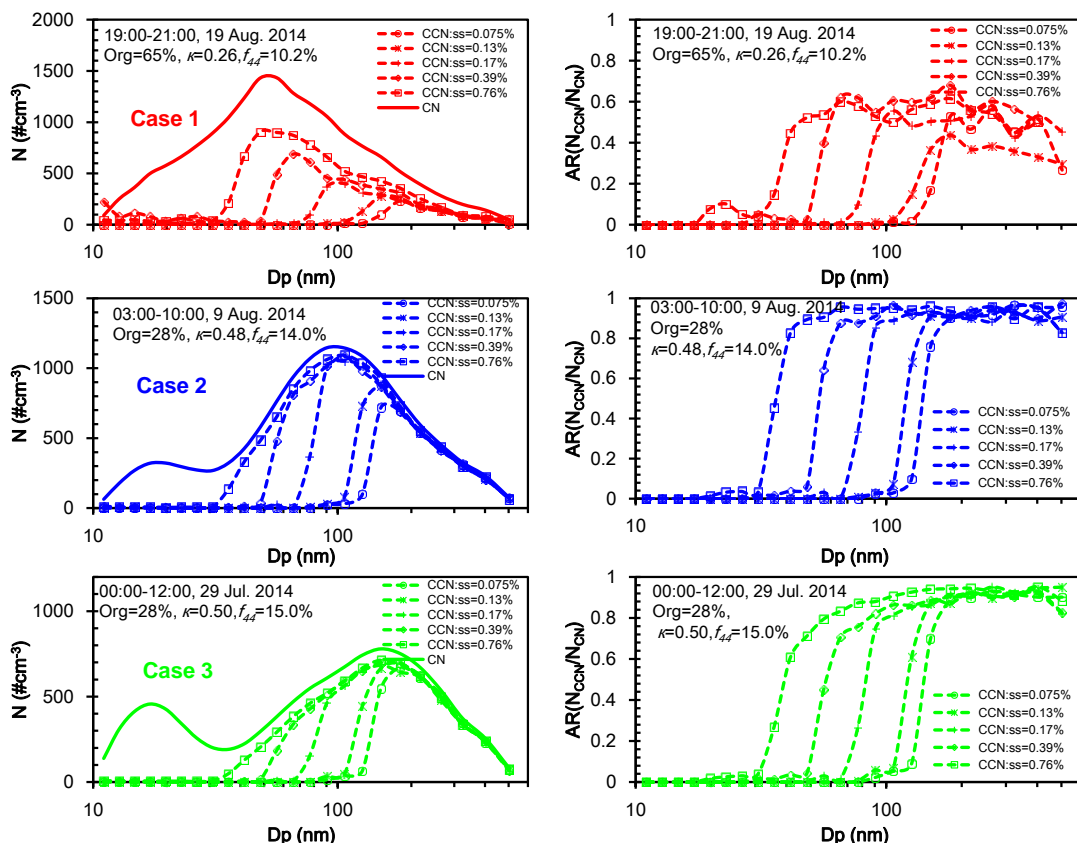
Figures



711  
712  
713  
714  
715  
716  
717  
718  
719  
720  
721  
722  
723  
724  
725  
726

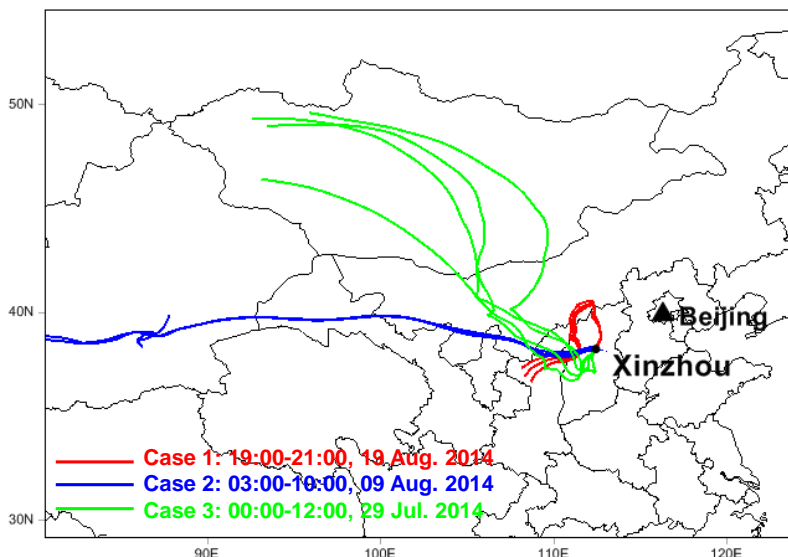
**Fig. 1.** Mean CCN efficiency spectra at the Xinzhou site (black lines with asterisks) measured from 22 July-26 August 2014 and at the Xianghe site (red lines with circles) site measured from 7-21 July 2013 for different supersaturation levels. Error bars representing one standard deviation are shown. Right panels show particle chemical composition in terms of mass concentration fractions at Xinzhou (top panel) and Xianghe (bottom panel) during their respective observation periods. The campaign average mass concentration of PM<sub>1</sub> is 31.6 μg m<sup>-3</sup> and 72.4 μg m<sup>-3</sup> at Xinzhou and Xianghe respectively. Note that the preset supersaturation levels were 0.07%, 0.1%, 0.2%, 0.4% and 0.8% at both sites, but effective supersaturation levels showed slightly different after calibration.





727  
728  
729  
730  
731  
732  
733  
734  
735  
736  
737  
738  
739  
740  
741  
742  
743  
744

**Fig. 2.** Particle number size distribution (PSD) and CCN size distributions (left panels) and CCN efficiency spectra (right panels) at different supersaturation levels for Case 1 (upper panels, 19 August 2014, 19:00-21:00 LT), Case 2 (middle panels, 9 August 2014, 03:00-10:00 LT), and Case 3 (bottom panels, 29 July 2014, 00:00-12:00 LT). CN number concentrations are  $16671 \text{ cm}^{-3}$ ,  $12869 \text{ cm}^{-3}$ , and  $10134 \text{ cm}^{-3}$  for Case 1, Case 2, and Case 3, respectively. Mass concentrations of  $\text{PM}_{10}$  are  $28.36 \mu\text{g m}^{-3}$ ,  $81.45 \mu\text{g m}^{-3}$ , and  $78.73 \mu\text{g m}^{-3}$  for Case 1, Case 2 and Case 3, respectively.



745

746 **Fig. 3.** Five-day back trajectories for Case 1 (in red), Case 2 (in blue), and Case 3 (in  
 747 green) calculated using the Hybrid Single-Particle Lagrangian Integrated Trajectory  
 748 model with National Centers for Environmental Prediction reanalysis data. The arrival  
 749 height of the trajectories at the Xinzhou site was at the surface.

750

751

752

753

754

755

756

757

758

759

760

761

762

763

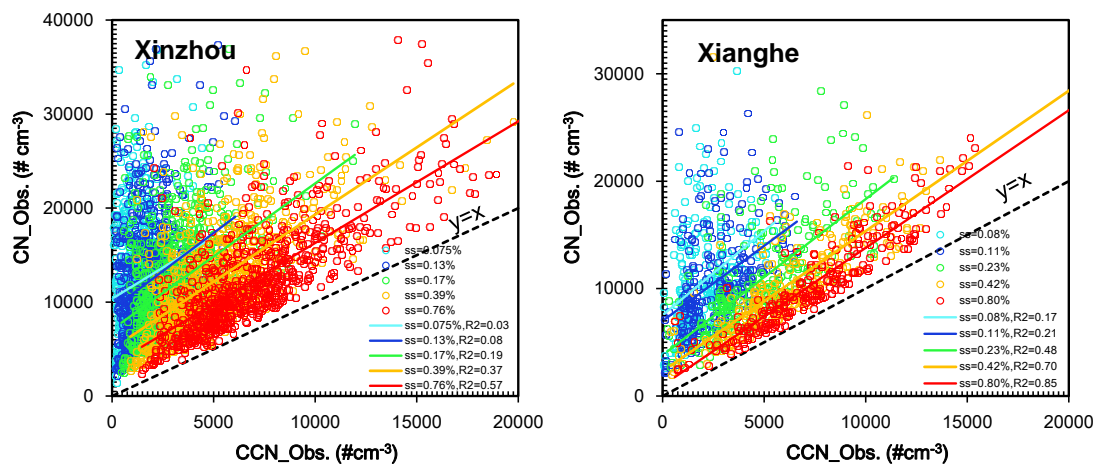
764

765

766

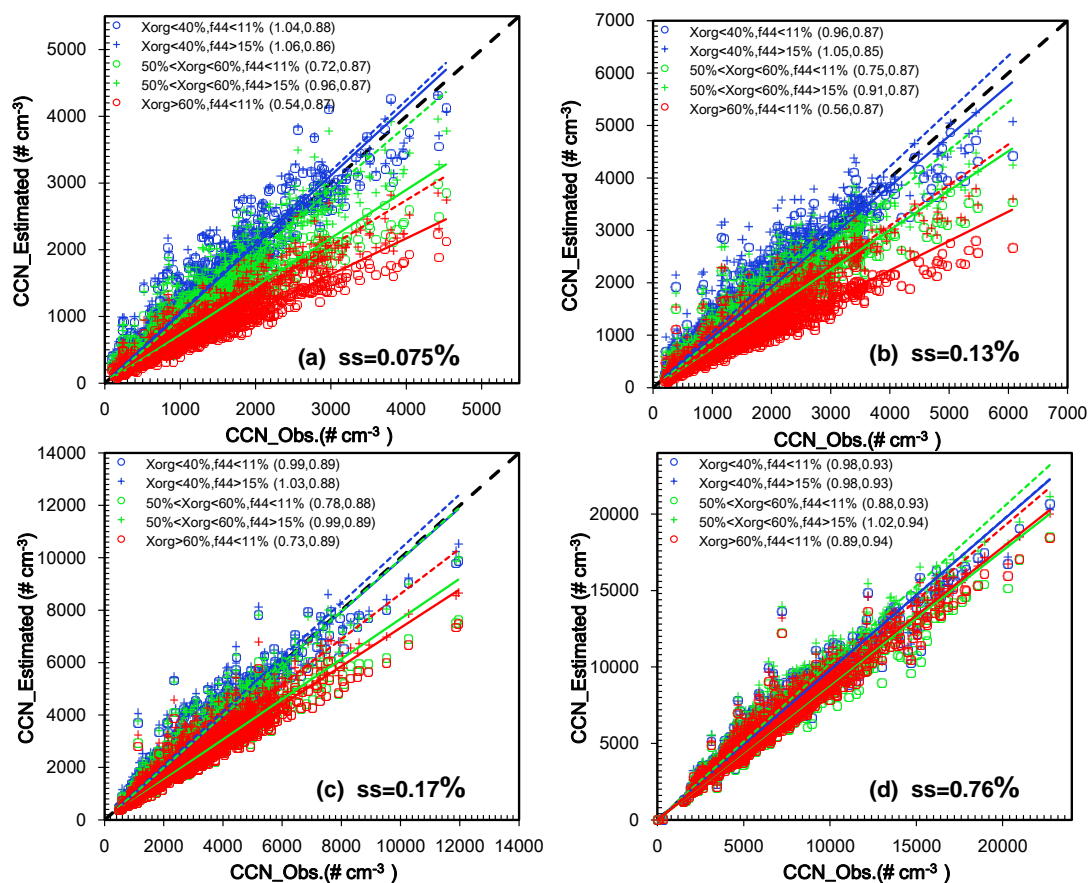
767

768



769  
 770  
 771  
 772  
 773  
 774  
 775  
 776  
 777  
 778  
 779  
 780  
 781  
 782  
 783  
 784  
 785  
 786  
 787  
 788  
 789  
 790  
 791  
 792  
 793  
 794  
 795

**Fig. 4.** Measured  $N_{CN}$  as a function of measured  $N_{CCN}$  for different supersaturation levels at the Xinzhou (left panel) and Xianghe (right panel) sites. The scatterplot between  $CCN_{Obs}$  and  $CN_{Obs}$  were fitted with a linear function (in colored lines) and  $R^2$  refer to the correlations of them.



796

797 **Fig. 5.** The sensitivity of organics volume fraction ( $x_{org}$ ) as well as oxidation level  
 798 (using  $f_{44}$ , the fraction of m/z 44 in total organics, as an indicator) of organics to  
 799 estimation of  $N_{CCN}$  at supersaturation levels of (a) 0.075%, (b) 0.13%, (c) 0.17% and  
 800 (d) 0.76%. for cases when  $x_{org} = 35\%$  (blue circles), 52% (green circles), and 66%  
 801 (red circles) The size-resolved CCN data were sorted when the  $x_{org} > 60\%$ ,  $50\% < x_{org}$   
 802  $< 60\%$ ,  $40\% < x_{org} < 50\%$  and  $x_{org} < 40\%$  respectively to do the sensitivity examination. The  
 803 results of  $40\% < x_{org} < 50\%$  was not plotted here. Mean values of the hygroscopic  
 804 parameter  $\kappa_{chem}$  at  $f_{44} < 11\%$  when  $x_{org} > 60\%$ ,  $50\% < x_{org} < 60\%$ ,  $40\% < x_{org} < 50\%$  and  $x_{org}$   
 805  $< 40\%$  are 0.27, 0.34, 0.40 and 0.46, respectively; while at  $f_{44} > 15\%$  the value  
 806 increased to 0.36, 0.42, 0.46 and 0.50 respectively. Linear best-fit lines through each  
 807 group of points are shown. Slopes and  $R^2$  values are given in parentheses.

808

809

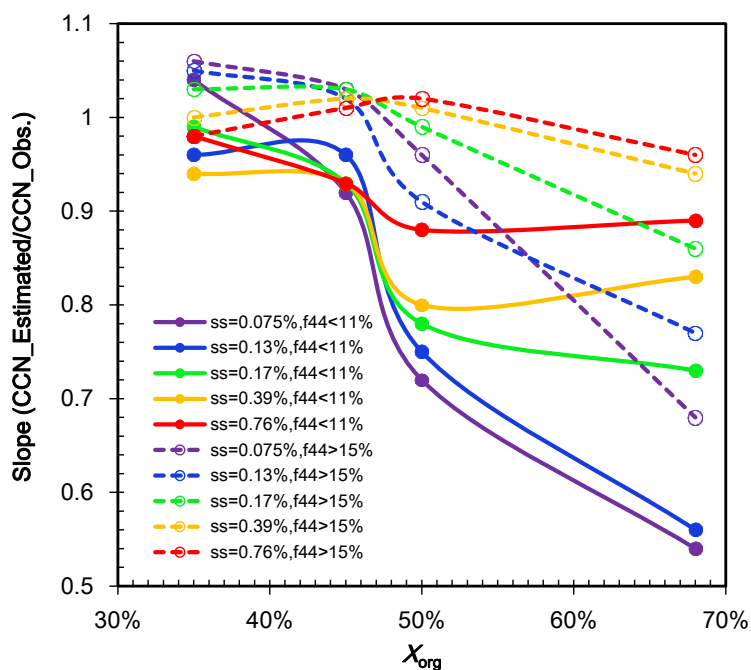
810

811

812

813

814  
815  
816  
817  
818  
819



820

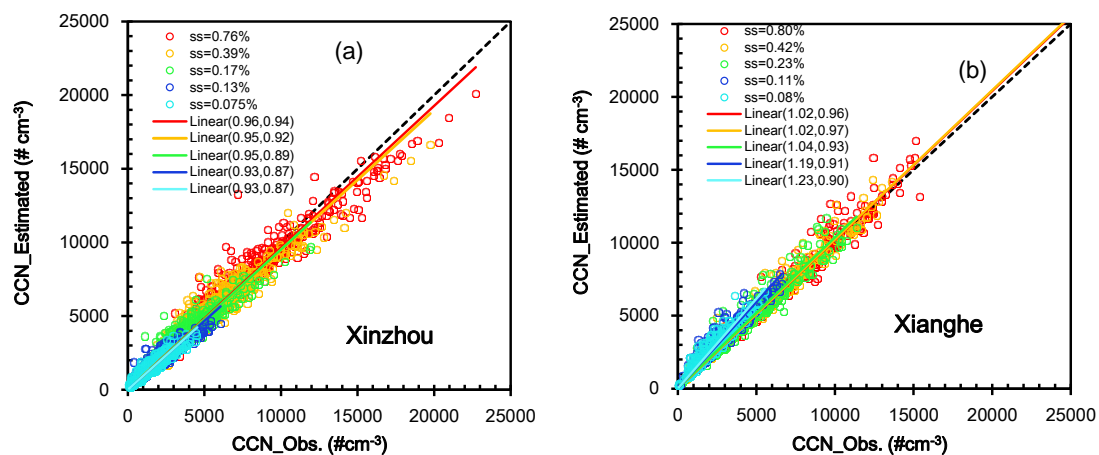
821 **Fig. 6.** Slopes of the linear fit of estimated and observed  $N_{CCN}$  dependence on volume  
822 fraction of organics ( $x_{org}$ ) at  $f_{44} < 11\%$  and  $f_{44} > 15\%$  for different supersaturation levels.

823  
824  
825  
826  
827  
828  
829  
830  
831  
832  
833  
834  
835

836

837

838



839

840

841 **Fig. 7.** Estimated  $N_{CCN}$  as a function of observed  $N_{CCN}$  for different supersaturation

842 levels at (a) Xinzhou and (b) Xianghe. Note that the campaign mean CCN efficiency

843 spectra at Xinzhou are used for estimating  $N_{CCN}$  at Xianghe. Linear best-fit lines

844 through each group of points are shown. Slopes and  $R^2$  values are given in

845 parentheses.

846

847

848

849

850

851

852